Analyst

Accepted Manuscript

ROYAL SOCIETY OF CHEMISTRY

www.rsc.org/analyst

Journal Name

RSCPublishing

ARTICLE

$CuFe_2O_4$ magnetic nanocrystal clusters as a matrix for the analysis of small molecules by negative-ion matrix-assisted laser desorption/ionization time-of-flight mass spectrometry

Cite this: DOI: 10.1039/x0xx00000x

Received 00th January 2012,
Accepted 00th January 2012

DOI: 10.1039/x0xx00000x

www.rsc.org/

Zian Lin,[ab]* Jiangnan Zheng,[b] Wei Bian,[a] and Zongwei Cai[a]*

$CuFe_2O_4$ magnetic nanocrystal clusters ($CuFe_2O_4$ MNCs) was proposed as a new matrix for small molecule analysis by negative ion matrix-assisted laser desorption/ionization time-of-flight mass spectrometry (MALDI-TOF MS) for the first time. We demonstrated its advantages over conventional organic matrices in the detection of small molecules such as amino acids, peptides, nucleobases, fatty acids, and steroid hormones. A systematic comparison of $CuFe_2O_4$ MNCs with different ionization modes revealed that MS spectra obtained on $CuFe_2O_4$ MNC matrix in negative ion mode was only featured by deprotonated ion peaks with free matrix background, which was different from the complicated alkali metal adducts produced in positive ion mode. The developed method was found relatively tolerant to salt contamination and good reproducibility. Detection limit down to subpicomolar level was achieved when testosterone was analyzed. In addition, by comparison of the MS spectra obtained from bare Fe_3O_4 and MFe_2O_4 MNC (M = Co, Ni, Cu, Zn) matrices, two main factors of MFe_2O_4 MNC matrices were unveiled to play a vital role in assisting negative ion desorption/ionization (D/I) process: doping transition metals into ferrite nanocrystals favoring laser absorption and energy transfer; good match between the UV absorption of MFe_2O_4 MNCs and the excitation of nitrogen laser source facilitating LDI efficiency. This work creates a new application branch for MFe_2O_4 MNCs and provides an alternative solution for small molecule analysis.

1. Introduction

Matrix-assisted laser desorption/ionization mass spectrometry (MALDI-MS) has become a powerful tool for bioanalysis since its debut by Karas et al. in the 1980s.[1] In MALDI-MS, analyte compounds are embedded in a surplus of matrix, consisting of small organic molecules (< 300 Da) with strong absorbance at the laser wavelength used, and are codesorbed upon laser excitation. Although MALDI-MS has proven to be very useful for the analysis of medium-size molecules (500-10 kDa) such as peptides, proteins, and oligosaccharides,[2–4] the analysis of low molecular-weight (LMW) compounds (< 500 Da) is far less successful than that of larger molecules because the analyte ions are strongly interfered with or are suppressed by the matrix-related ions that are predominant at the low-mass range.[5,6] In addition, the heterogeneous cocrystallization of analytes with a matrix, such as α-cyano-4-hydroxycinnamic acid (CHCA), requires sweet-spot searching, which leads to poor shot-to-shot reproducibility.[7,8]

The problems associated with so-called "sweet spots" and "high background noise" are minimized when nanomaterials are used as matrices, rather than the organic matrices employed in MALDI-MS; this approach is often called surface-assisted laser desorption/ionization mass spectrometry (SALDI-MS).[9] Up to now, a variety of inorganic nanoparticles with different composition and morphology, including porous silicon,[10,11] metal nanoparticles,[12–14] metal oxide,[15,16] carbon-based materials,[17–20] as well as metal-organic frameworks[21] have been explored to be effective MALDI matrices. Among various candidates, metal and metal oxide nanoparticles (e.g. Au[22], Ag,[23] TiO_2,[24,25] Fe_3O_4,[16,26,27] CdSe,[28] and HgTe[29]) exhibit strong UV absorption and have been actively investigated for use in SALDI-MS. Compared with metal nanoparticles, metal oxide nanoparticles usually provide better stability, sensitivity, and less metal cluster ions as SALDI matrices. However, most current analysis of LMW compounds using metal/metal oxide nanoparticle matrices has generally been determined in positive ion mode in which the analytes are easily ionized as multiple alkali metal adducts, while scant attention has been paid to negatively charged ions. Theoretically, the negative ion spectrum is much clearer and easier to interpret with only one

deprotonated ion peak present.[30,31] Furthermore, recent works also confirm that better sensitivity can be obtained in negative ion mode than in positive ion mode for analytes such as amino acids, glyans, fatty acid, and peptides.[19,20,32–34] Given the advantages of negative ion mode for small molecule analysis, discovering negative ion mode compatible matrices and improving the LDI efficiency by optimization are of crucial significance for sensitive MALDI-MS readout of low molecular-weight compounds.

Nanoparticles of spinel ferrites with the general formula MFe_2O_4 (M = Co, Ni, Cu, Zn) are of long-standing interest due to their theoretical and technological relevance.[35,36] Of the MFe_2O_4 materials, nanocrystalline copper ferrites ($CuFe_2O_4$) exhibit excellent electronic, magnetic, and catalytic properties, and thus have been widely applied in the fields of electronics and catalysis.[37,38] More recently, our group[39] proposed a facile approach for synthesis of $CuFe_2O_4$ magnetic nanocrystal clusters ($CuFe_2O_4$ MNCs) and first applied it in bioseparation. In principle, by virtue of the unique nanostructure, electronic and magnetic properties, $CuFe_2O_4$ MNCs is an ideal candidate for SALDI matrix. However, no reports on the applications and in-depth mechanism study of $CuFe_2O_4$ MNCs in MS technology have been explored so far.

In this paper, we prepared $CuFe_2O_4$ MNCs via a facile one-pot hydrothermal approach and first introduced it as a matrix for negative ion MALDI-TOF MS of small molecules. A comparison of $CuFe_2O_4$ MNCs with different organic matrices and ionization modes revealed that the $CuFe_2O_4$ MNCs in negative ion mode can provide free matrix background in the analysis of peptides, amino acids, fatty acids, nucleobases and steroid hormones. The in-depth mechanism study on negative ion mode was also discussed in detail.

2. Experimental

2.1 Chemicals and materials

All other chemicals were of analytical grade or better. Six peptides (Tyr-Gly-Gly, Tyr-Phe, Glu-Val-Phe, Phe-Gly-Phe-Gly, Tyr-Gly-Gly-Phe-Leu, and Arg-Ser-Gly-Phe-Tyr) were purchased from Shanghai Apeptide Co. Ltd (Shanghai, China). Amino acids (glycine (Gly), aspartic acid (Asp), glutamine (Gln), histidine (His), phenylalanine (Phe), tyrosine (Tyr) and tryptophan (Trp)), nucleobases (cytosine (C), thymine (T), adenine (A) and guanine (G)), 17β-estradiol (E2) and testosterone (Te) and α-cyano-4-hydroxycinnamic acid (CHCA) were obtained from Sigma-Aldrich (St. Louis, MO). 3-Aminoquinoline (5-AQ) was purchased from Fluka (Buchs, Switzerland). Saturated fatty acids including *n*-dodecanoic acid (C12), *n*-tetradecanoic acid (C14), *n*-hexadecanoic acid (C16), *n*-octadecanoic acid (C18) and *n*-eicosanoic acid (C20) were obtained from Acros Organics (New Jersey). Methanol (MeOH) and acetonitrile (ACN) were of HPLC grade and supplied by TEDIA (Fairfield, OH). Peptide calibration standard used for calibration of TOF-MS instrument was obtained from Bruker Daltonics (Bruker, Germany). Scanning electron microscopy (SEM) images were obtained using a Hitachi S-4800 TEM (Japan). Transmission electron microscopy (TEM) analyses were performed on a FEI Tecnai G2 20 (USA) at 200 kV. Urine was collected from a healthy adult male volunteer. Deionized water (18.2 MΩ cm^{-1}) was prepared with a Milli-Q water purification system (Millipore, USA).

2.2 Synthesis of MFe_2O_4 MNCs and Fe_3O_4 MNCs.

$CuFe_2O_4$ MNCs were prepared by a solvothermal reaction as described in our previous work.[39] Briefly, $FeCl_3 \cdot 6H_2O$ (4.050 g), $CuCl_2 \cdot 2H_2O$ (1.278 g), NaAc (8.2 g), and $Na_3Cit \cdot 2H_2O$ (29.4 mg) were dissolved in ethylene glycol (100 mL). The obtained solution was transferred to autoclave, and then heated to 200 °C for 12h. Afterward, the product was washed several times with water and ethanol and dried. Similarly, $CoFe_2O_4$, $NiFe_2O_4$ and $ZnFe_2O_4$ MNCs were also prepared by replacing $CuCl_2 \cdot 2H_2O$ with $Co(NO_3)_2 \cdot 6H_2O$ (2.1827 g), $NiCl_2 \cdot 6H_2O$ (1.782 g), and $ZnCl_2$ (1.022 g), respectively. For comparison, bare Fe_3O_4 MNCs were also prepared in the absence of $CuCl_2 \cdot 2H_2O$.

For comparison, bare Fe_3O_4 MNCs were also prepared in the absence of $CuCl_2 \cdot 2H_2O$. Briefly, $FeCl_3 \cdot 6H_2O$ (6.081 g, 22.5 mmol), NaAc (8.2 g, 100 mmol), and $Na_3Cit \cdot 2H_2O$ (29.4 mg, 0.1 mmol) were dissolved in ethylene glycol (100 mL). The obtained homogeneous solution was transferred to autoclave, and then heated to 200 °C for 12h. In parallel, the product was rinsed with water and ethanol for several times and dried at room temperature.

2.3 Preparation of analyte solution

Gly, Asp, Gln, His and Phe were respectively dissolved in water at a concentration of 10 mM as stock solutions. Tyr and Trp were dissolved in water/formic acid (1:1, v/v) at a concentration of 10 mM at stock solution. All of peptides were respectively dissolved in water/MeOH (1:1, v/v) at a concentration of 5 mM as stock solution. C and A were respectively dissolved in hot water at a concentration of 10 mM as stock solutions. T and G were dissolved in hot water/formic acid (1:1, v/v) at a concentration of 5 mM at stock solution. Fatty acids of C12, C14, C16, C18 and C20 were dissolved in anhydrous ethanol at a concentration of 10 mM as stock solutions. E2 and Te were dissolved in methanol at a concentration of 10 mM as stock solutions. All analyte solutions were stored at 4 ℃ for use.

Human urine sample used here was collected from a healthy adult male volunteer according to the standard clinical procedures. In this case, the urine samples spiked with different concentration Te were prepared by adding 1μL and 0.1 μL of Te (1.0 mM) into 10 μL urine respectively. Afterward, the above solution was diluted with ACN to 1 mL. Next, the mixtures were shaken for 5 min, followed by centrifugation at 5000 rpm for 5 min. finally, 1 μL clear supernatant was pipetted for MALDI-TOF MS analysis.

2.4 Sample preparation for MALDI-TOF MS analysis.

CHCA (10 mg mL^{-1}) matrix was dissolved in ACN and 0.1% aqueous TFA at a ratio of 2:1. 3-Aminoquinoline (3-AQ) was

dissolved at in ACN/H_2O (1:1) at 10 mg mL^{-1}. $CuFe_2O_4$ MNCs were dispersed in ethanol/H_2O (1:1, v/v) and sonicated for 5 min to form homogeneous suspension solutions (1 mg mL^{-1}). Subsequently, 1 μL matrix was first pipetted on the target plate, and air-dried, followed by 1 μL analyte solution (0.5 μL for fatty acids).

2.5 MALDI-TOF MS analysis.

All experiments were performed both in positive- and negative- ion modes on identical samples and identical instrument settings (Bruker Autoflex Ⅱ mass spectrometer, Bruker Daltonics, Germany), and all data were automatically acquired by AutoXecute acquisition control software. Nitrogen laser operated at 337 nm and laser attenuator offset of ~67% in positive and negative reflection mode were applied. Acquisition parameters included 19 kV acceleration voltages and delayed extraction at 120 ns. Each recorded mass spectrum was generated by averaging data from 500 individual laser shots. In order to avoid fragmentation of the analytes, the laser power was adjusted to slightly above the D/I threshold energy. Mass calibrations were performed externally using the mass peaks of CHCA and 2,5-dihydroxybenzoic acid (DHB) for small molecule analysis.

3. Results and discussion

3.1 Characterization of $CuFe_2O_4$ MNCs

The $CuFe_2O_4$ MNCs was synthesized by a facile one-pot hydrothermal route, which has been described and characterized in our previous work.[39] Representative SEM image showed that the synthesized $CuFe_2O_4$ MNCs were nearly uniform with good monodispersity and had an average diameter of 170 nm (Figure.1(A)). TEM image validated the $CuFe_2O_4$ MNCs was composed of nanocrystals with a small size of about 6-15 nm (Figure.1(B) and the inset). Generally, the good reproducibility is strongly dependent on the homogeneous distribution of the matrix/analyte mixture that results in a good shot-to-shot yield. However, the inhomogeneous cocrystallization of organic matrix with analytes was observed in Figure.S1(A-B) (Supporting Information), which caused hot spots and thereby required sweet-spot searching. In contrast, $CuFe_2O_4$ MNC matrix prevented the formation of this problem and Figure.S1(C) (Supporting Information) proved to be the outstanding homogeneous distribution of the matrix/analyte mixture, which made it possible for obtaining good shot-to-shot reproducibility.

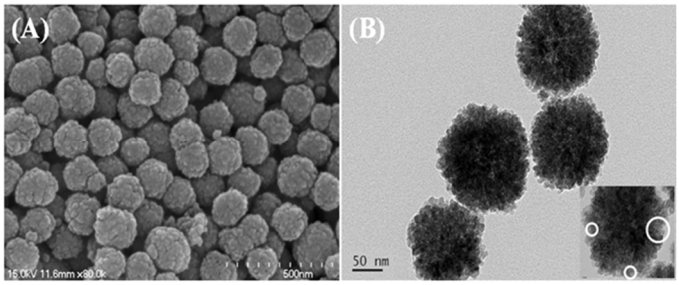

Figure 1. SEM (A) and TEM (B) images of $CuFe_2O_4$ MNCs (high-magnification TEM image in down-right inset)

3.2 Effect of Concentration of $CuFe_2O_4$ MNCs

It is well known that the concentration of matrix has a great effect on the MS signal of analytes in MALDI-MS. As a result, the effect of $CuFe_2O_4$ concentrations from 0.5 to 2.0 mg mL^{-1} was investigated in negative ion mode using Phe as a model sample. As shown in Figure.2, a deprotonated $[M-H]^-$ ion of Phe with signal-to-noise (S/N) ratio of 24 and 30.2 was obtained while using 0.5 mg mL^{-1} and 1.0 mg mL^{-1} $CuFe_2O_4$ MNCs, respectively. At concentration of 2.0 mg mL^{-1}, the MS signal of Phe increased with S/N of 47.7, but background noise originated from matrix cluster peaks also increased accordingly. As a compromise, the concentration of $CuFe_2O_4$ MNCs with

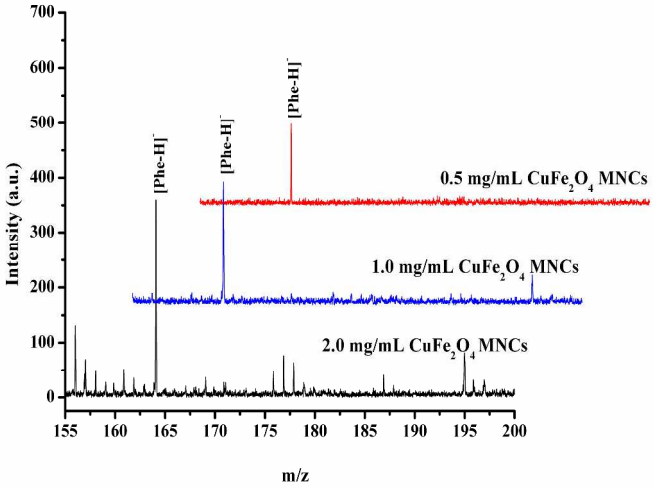

1.0 mg mL^{-1} was selected as the best for further studies.

Figure 2. Mass spectra of 0.1 mM Phe obtained by using $CuFe_2O_4$ MNCs as matrix with different concentration. (laser intensity of 55%)

3.3 MALDI-TOF MS of amino acids

In the preliminary application test, a solution including Gly (MW=75.07), Asp (MW=133.11), Gln (MW=146.14), His (MW=155.15), Phe (MW=165.19), Tyr (MW=181.19) and Trp (MW=204.23) was analyzed by MALDI-TOF MS using CHCA, 3-AQ, and $CuFe_2O_4$ MNCs as matrices in both positive and negative modes. As shown in Figure.3(A), when CHCA matrix was applied in positive ion mode, the $[M+H]^+$ ions of all amino acids except Asp and the $[M+Na]^+$ ions of Asp (m/z 156.03) and Phe (m/z 188.02) were detected at fairly low intensity, and its fragments dominated the spectrum, seriously suppressing analyte signals. However, there were only matrix-related ions ($[M-H]^-$ at m/z 188.02 and $[M-CO_2-H]^-$ at m/z 144.01) but no analyte signals were detected (data not shown) in negative ion mode, implying the infeasibility of CHCA in assisting negative ionization. As an alternative, 3-AQ was applied in negative ion mode.[40] Although the deprotonated $[M-H]^-$ ions of all amino acids except Gly were obtained, the MS response of the amino acids was rather low (Figure.3(B)). Moreover, the matrix-related ions with high signal intensity

dominated the spectra in low-mass region, making it difficult for identification. By using $CuFe_2O_4$ MNCs, however, multiple amino acid-related positive ions were observed (Figure.3(C)), where the $[M+Na]^+$ and $[M+K]^+$ ions of all amino acids were reflected in the spectra, corresponding to Gly (98.04, 114.01), Asp (156.05, 172.04), Gln (169.07, 185.04), His (178.08, 194.06), Phe (188.09, 204.07), Tyr (204.07, 220.05) and Trp (227.09, 243.08). Apparently, the complicated mass spectra obtained in positive ion mode make it difficult for identification and interpretation. In comparison with positive ion mode, negative ion mode provides clean background for detection of the amino acids and the result was shown in Figure.3(D). The only characteristic $[M-H]^-$ ions of seven amino acids at m/z 74.01, 131.99, 145.03, 154.04, 164.06, 180.05, and 203.07 predominated the negative ion spectra. Compared with the Pt- and TiO_2-based nanomatrices in negative ion mode,[41,42] the $CuFe_2O_4$ MNCs exhibited wider adaptability for amino acid detection. Meanwhile, the result can stand comparison with those using graphene- and N-doped graphene matrices,[19,20] in which the deprotonated ions of amino acids were obtained with clean background. Moreover, the MS signal intensities of amino acids with $CuFe_2O_4$ MNCs matrix were higher than those obtained in 3-AQ matrix under the same experimental conditions (Table S1, Supporting Information), demonstrating its superiority over organic matrices.

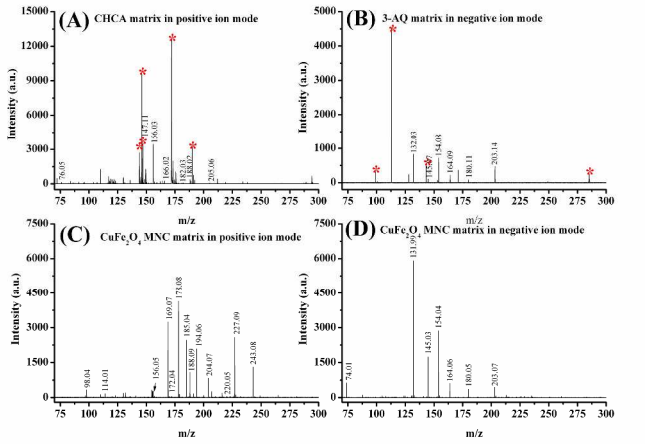

Figure 3. Mass spectra of seven amino acids by using. (A) CHCA matrix in positive ion mode; (B) 3-AQ matrix in negative ion mode; (C) $CuFe_2O_4$ MNC matrix in positive ion mode and (D) negative ion mode. The concentration of all analytes was set as 1mM. Laser intensity: 55%. Red asterisk is background peaks of matrix unless otherwise noted.

3.4 MALDI-TOF MS of peptides

Although CHCA and DHB are the most commonly used matrices for peptide analysis by MALDI-MS, their signals would be located at the m/z range of matrix and compromised by matrix background. In this experiment, six peptides of Tyr-Gly-Gly (MW=295.12), Tyr-Phe (MW=328.14), Glu-Val-Phe (MW=393.19), Phe-Gly-Phe-Gly (MW=426.19), Tyr-Gly-Gly-Phe-Leu (MW=555.27) and Arg-Ser-Gly-Phe-Tyr (MW=628.69) was first individually analyzed by MALDI-TOF MS with CHCA and 3-AQ. Only three peptides were detected with CHCA in positive ion mode, and the corresponding peaks were assigned to $[M+Na]^+$ and $[M+K]^+$ for Phe-Gly-Phe-Gly, $[M+Na]^+$, $[M+K]^+$, $[M+2Na-H]^+$, and $[M+Na+K-H]^+$ for Tyr-Gly-Gly-Phe-Leu, and $[M+H]^+$ for Arg-Ser-Gly-Phe-Tyr (Figure.4(A)). Switching to negative ion mode, four peptides were detectable as the deprotonated ion form (Figure.4(B)), but with fairly low response. A comparison between Figure.4(C) and (D) demonstrated that only three peptides (Glu-Val-Phe, Tyr-Gly-Gly-Phe-Leu and Arg-Ser-Gly-Phe-Tyr) were detected by using 3-AQ matrix in negative ion mode. With the $CuFe_2O_4$ MNCs, however, all of peptides except Arg-Ser-Gly-Phe-Tyr were well detected in the form of $[M+Na]^+$ and $[M+K]^+$ ions under positive ion mode, in addition to the $[M+Na+K-H]^+$ ion for Phe-Gly-Phe-Gly (Figure.4(E)). More detailed peak identification of the peptides was listed in Table S2 (Supporting Information). Different from positive ion mode, negative ionization is an ideal solution to avoid the adduct ions and clarify the spectrum. As expected, the deprotonated ions of the five former peptides yielded strong signals at m/z 294.02, 327.32, 392.49, 425.55, and 554.86 were obtained in the negative ion spectra (Figure.4(F)), and their corresponding MS signal intensities were listed in Table S3 (Supporting Information). It should be noted that the $[M-H_2O-H]^-$ peak was observed for Arg-Ser-Gly-Phe-Tyr, due to water loss from Ser. Nevertheless, the characteristic ions of the peptides with clean

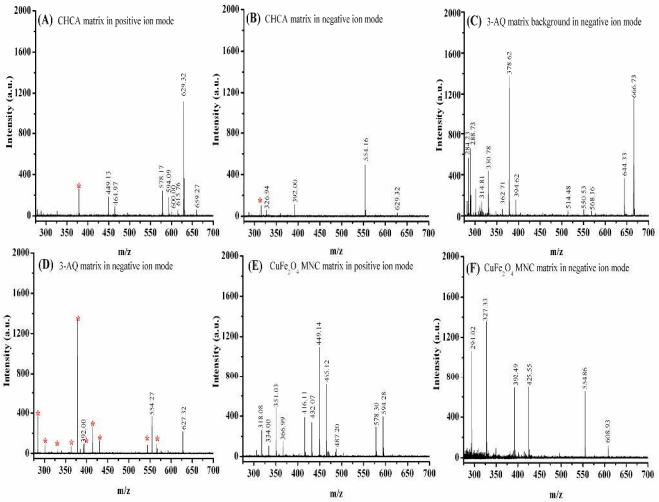

background were achieved in negative ion mode.

Figure 4. Mass spectra of six peptides by (A) CHCA matrix in positive ion mode, and (B) negative ion mode; (C) 3-AQ matrix blank, and (D) 3-AQ matrix in negative ion mode; (E) $CuFe_2O_4$ MNC matrix in positive ion mode, and (F) negative ion mode. The concentrations of Tyr-Gly-Gly, Tyr-Phe, Glu-Val-Phe, Phe-Gly-Phe-Gly, Tyr-Gly-Gly-Phe-Leu and Arg-Ser-Gly-Phe-Tyr were adjusted to 0.8, 0.75, 0.75, 0.75, 0.9, and 0.8 mM, respectively. Laser intensity: 65%.

3.5 MALDI-TOF MS of nucleobases.

Four nucleobases (C, T, A and G) was further tested. With CHCA in positive ion mode, only three nucleobases (C, A and G) could be detected as $[M+H]^+$, $[M+Na]^+$, $[M+K]^+$, and $[M+Na+K-H]^+$, which was presented in Figure.5(A) and Table S4 (Supporting Information). Among them, two of the analyte peaks ($[C+Na+K-H]^+$ and $[G+K]^+$) were overlapped with the

fragments of CHCA, resulting in difficult identification. Oppositely, only two nucleobases (A and T) were observed at m/z 125.04 and m/z 134.06 (Supporting Information Figure.S2) in negative ion mode. Similar result (Figure.5(B)) was obtained while using 3-AQ matrix in negative ion mode. However, all four nucleobases can be well detected with $CuFe_2O_4$ MNCs. Presented in Figure.5(C) (and Table S5 in Supporting Information) was the positive ion analysis of four nucleobases, where the $[M+Na]^+$, $[M+K]^+$, and $[M+Na+K-H]^+$ ions of the nucleobases dominated the spectrum with low intensity. Compared to positive ion mode, the negative ion mode of $CuFe_2O_4$ MNCs gave a clean background and the exclusive $[M-H]^-$ ions of the four analytes were clearly observed (Figure.5(D)), revealing the superiority of $CuFe_2O_4$ MNCs as matrix.

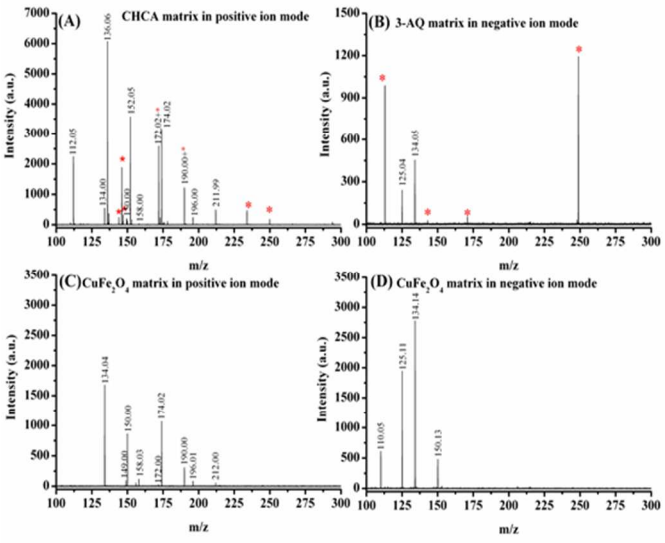

Figure 5. Mass spectra of four nucleobases by using (A) CHCA matrix in positive ion mode; (B) 3-AQ matrix in negative ion mode; (C) $CuFe_2O_4$ MNC matrix in positive ion mode and (D) negative ion mode. The concentration of all analytes was set as 1mM. Laser intensity: 55%.

3.6 MALDI-TOF MS of fatty acids

It is underscored by the fact that none of the selected standard fatty acids were detected with CHCA or 3-AQ in either positive ion mode or negative ion mode (data not shown). Here we applied these species as the analytes in both positive and negative ion modes to assess the performance of $CuFe_2O_4$ MNC matrix. As shown in Figure.6(A), the $[M+Na]^+$ and $[M+2Na+K]^+$ ions of all five fatty acids were detected in positive ion mode, corresponding to C12 (221.12, 285.11), C14 (251.14, 313.13), C16 (279.16, 341.17), C18 (307.18, 369.21), and C20 (335.22, 397.25). However, in negative ion mode, the deprotonated $[M-H]^-$ ions of fatty acids were obtained with high S/N ratios (Figure.6(B)). The result was well in accordance with the use of graphene-based nanomatrices,[19,20] but better than porous silicon matrix,[43] and colloidal graphite-based matrix,[18] because both of the latter gave rise to $[M-H]^-$ ions as well as different alkali cationized deprotonated multimers[43] or a few low-number carbon cluster ions.[18]

In the assessment of salt tolerance (Supporting Information Figure.S3), addition of NaCl below 1000 mM had slight influence on the signal intensities of the fatty acids. While the concentration of NaCl was raised by 3 orders of magnitude, the MS signals of fatty acids witnessed a decline by less than 20% of the initial intensity. Nevertheless, the five fatty acids could be clearly detected with decent S/N ratios in the ranges of 25-70, indicating its good tolerance towards high salt concentration.

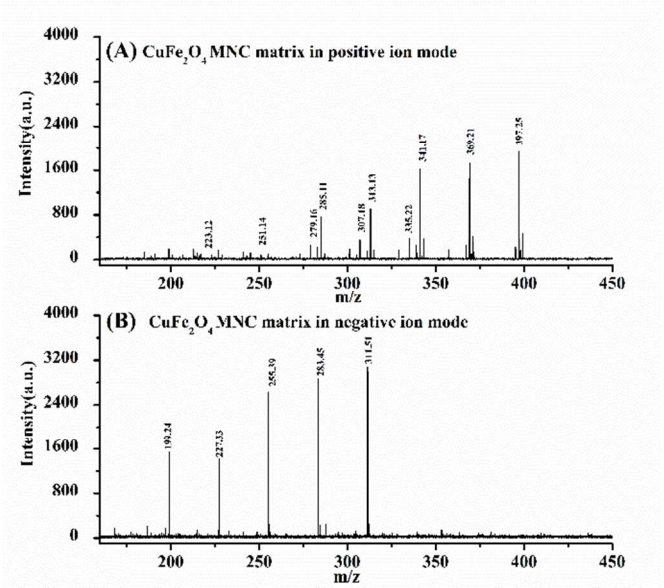

Figure 6. Mass spectra of fatty acids. (A) $CuFe_2O_4$ MNC matrix in positive ion mode, and (B) in negative ion mode. The concentration of all analytes was set as 1mM. Laser intensity: 60%.

3.7 Signal reproducibility

The reproducibility is an important factor for the effectiveness of the proposed method. In current study, 0.1 mM of Phe was used as model molecule to examine the MS signal reproducibility. For the same sample spot detection, the MS signal intensity of 20 acquisition times was stabilized at around 178 with the relative standard deviation (RSD) of 12.1 % (n=20) (Supporting Information Figure.S4(A)). Even in the present of 1000 mM NaCl, the RSD of the signal intensity for Phe was less than 28.5% (n=20), demonstrating the good shot-to-shot reproducibility. In addition, the signal from different spots also exhibited good reproducibility with RSD of 12.8%. (n=10) (Supporting Information Figure.S4(B)). The good reproducibility can be attributed to the uniform structure of $CuFe_2O_4$ MNCs and homogeneous distribution of the matrix/analyte crystals. It is worth noting that the RSD values were much lower than the previous reports obtained with CHCA, where the RSDs of shot-to-shot and spot-to-spot reproducibility were usually higher than 60%.[44]

Sensitivity is an important indicator for measuring the practicality of the analytical method. In this case, Phe was

selected for the sensitivity evaluation and higher laser energy (70%) was recommended in order to obtain lower detection limit. As expected, the signal intensity and S/N ratio of Phe were accordingly decreased with the decreasing concentration (data not shown). The $[M-H]^-$ peak of Phe could be observed with the S/N ratio of 11.1 (Supporting Information Figure.S5), even when 5 μM sample (equivalent to 5 pmol) was used, demonstrating its feasibility of quantitative analysis.

3.8 MALDI-TOF MS analysis of sex steroid hormones

Sex steroid hormones, especially for E2 and Te, are the most important species of endogenous metabolites. Monitoring E2 or Te will play a vital role in understanding disease progression. Employing E2 (MW = 272.18) and Te (MW = 288.20) as the model analytes, we further tested the applicability of $CuFe_2O_4$ MNC matrix in the analysis of steroid hormones. As shown in Figure.7(A-B), E2 and Te were respectively detected as only deprotonated $[M-H]^-$ ions at m/z 271.22 and 287.15 with the assistance of $CuFe_2O_4$ MNC matrix. It should be pointed out that an unknown peak (m/z 254.5) was observed in the analysis of Te. It is suspected that the unknown ion may be originated from the impurity of Te standard. Nevertheless, the $[M-H]^-$ peaks of E2 and Te can be detected with a high S/N ratios of 45.6 and 52.9, even at a low concentration (0.1 mM for E2 and Te). The above attempts in detection of E2 and Te based on $CuFe_2O_4$ MNC matrix gave us more confidence for exploring its application potential in complex biological sample.

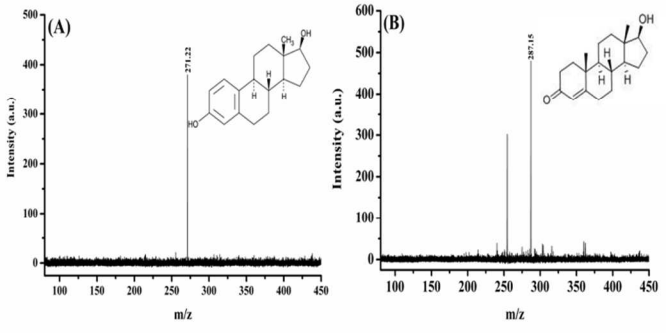

Figure 7. Mass spectra of sex steroid hormones (A) E2 and (B) Te by using $CuFe_2O_4$ MNC matrix in negative ion mode. The concentration of all analytes was set as 0.1mM. The laser intensities of 65% and 70% were applied for E2 and Te, respectively.

3.9 Analysis of testosterone in human urine.

Figure.S6 (Supporting Information) represented the quantitative analysis of Te with different concentrations (from 0.1μM to 100 μM). A linear relationship was found between the ion intensity of Te and its concentration in the range of 1 to 100 μM and the regression equation was y = 3.964x + 79.999 (R^2 = 0.9912) (Supporting Information Figure.S7). The characteristic peak of Te could still be detected with S/N ratio of 8.4, even in the case of 0.1μM (equivalent to 0.1 pmol). In addition, MALDI-TOF MS with $CuFe_2O_4$ MNCs as matrix was adopted to determine Te in the spiked human urine sample. Figure.8 presented the MS peaks of the blank urine and Te in spiked

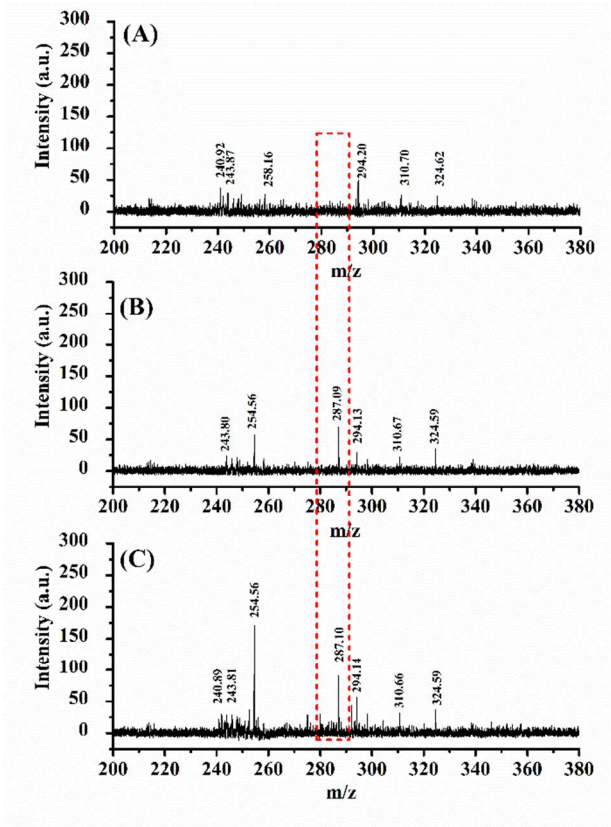

urine. No Te was detected in the blank urine. After spiking Te with 1.0 μM and 0.1μM, the unambiguous $[M-H]^-$ ions of Te were observed with S/N ratios of 12.4 and 9.6, respectively. The signal intensities of Te in the spiked urine were comparable to those in standard test solution (Figure.S6, Supporting Information), exhibiting its good resistance to the complex substrate of real sample.

Figure 8. Mass spectra of Te. (A) Blank urine, (B) 0.1 μM; (C) 1 μM in spiked urine by using $CuFe_2O_4$ MNC matrix in negative ion mode. Laser intensity: 70%.

3.10 General applicability of metal ferrite-assisted MALDI-TOF MS and mechanism study.

To evaluate the general applicability, metal ferrite-assisted LDI MS using bare Fe_3O_4 MNCs and MFe_2O_4 MNCs (M = Co, Ni, Cu, Zn) were systematically investigated and compared by analyzing fatty acids. The result was shown in Figure.S9 (Supporting Information). Using the bare Fe_3O_4 MNCs as matrix, the five fatty acids were detected with very low intensity and their corresponding S/N ratios were ranged from 9.7 to 23.2. Oppositely, remarkably improved signal enhancement by 2- to >20-fold were obtained while using MFe_2O_4 MNCs (M = Co, Ni, Cu, Zn) as matrices, suggesting the general applicability of using MFe_2O_4 MNCs as SALDI matrices. Although the detailed mechanism is unknown, it seems probable that transition metals- doped ferrite nanocrystals are endowed with the unique electronic property, which favoured laser absorption and energy transfer.[45]

Based on the above results, we attempted to elucidate the principle how the variation of metal composition influenced its efficacy in inducing ionization from another point of view. Figure.9 showed the UV-visible spectra of the MFe_2O_4 and bare Fe_3O_4 suspension solution. The MFe_2O_4 suspension, in general, showed stronger adsorption coefficient at or near the wavelength of 337 nm than the bare Fe_3O_4 suspension (λ_{max} = 605 nm), which matched well with the emission wavelength of the irradiation source (laser, 337 nm). Therefore, the MFe_2O_4 MNCs could effectively transfer photon energies absorbed from UV laser light. Although the exact mechanism of LDI in SALDI-based systems is yet not completely understood, we believe that transition metal substitution and UV/Vis adsorption are two non-ignorable reasons for the enhanced MS responses.

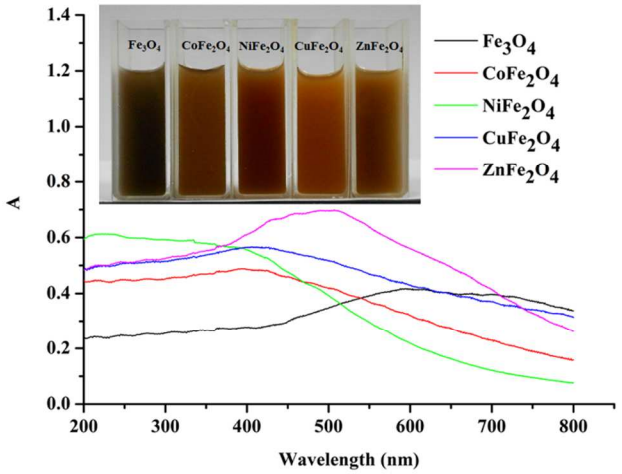

Figure.9 UV-Visible spectra of the MFe_2O_4 and bare Fe_3O_4 suspension solution. Inset photo: visual color change of the MFe_2O_4 and bare Fe_3O_4 suspension solution. The concentration of all analytes was set as 1.0 mg mL^{-1} for UV detection and 0.33 mg mL^{-1} for photo.

4. Conclusions

In summary, we have proposed a new matrix, $CuFe_2O_4$ MNCs, and investigated its abilities for the detection of small molecules in negative ion MALDI-TOF MS. Satisfactory MS responses were obtained in the analysis of amino acids, peptides, nucleobases, fatty acids as well as steroid hormones. Compared to organic matrices, $CuFe_2O_4$ MNCs exhibited many advantages, including interference-free background, high salt tolerance, and good reproducibility, which made it a very promising SALDI matrix. In addition, the preliminary results showed the general applicability of the MFe_2O_4 MNCs as SALDI matrices and the UV-Visible spectra also revealed that the MFe_2O_4 MNCs can enhance the MS signals of the analytes in negative ionization with respect to bare Fe_3O_4 MNCs. It is believed that the MFe_2O_4 MNC-assisted LDI-TOF MS would be an alternative tool to solve more analytical challenges.

Acknowledgements

We gratefully acknowledge the financial support from the National Natural Science Foundation of China (21375018 and 21175025), and the Natural Science Foundation of Fujian Province (2014J01402).

Notes and references

[a] Partner State Key Laboratory of Environmental and Biological Analysis, Department of Chemistry, Hong Kong Baptist University, 224 Waterloo Road, Kowloon Tong, Hong Kong, SAR, P. R. China
[b] Ministry of Education Key Laboratory of Analysis and Detection for Food Safety, College of Chemistry, Fuzhou University, Fuzhou, Fujian, 350116, China
Electronic Supplementary Information (ESI) available: Experimental details and additional figures. See DOI: 10.1039/c0xx00000x

1 M. Karas, D. Bachmann, U. Bahr and F. Hillenkamp, *Int. J. Mass Spectrom. Ion Process.*, 1987, **78**, 53–68.
2 D. P. Magparangalan, T. J. Garrett, D. M. Drexler and R. A. Yost, *Anal. Chem.*, 2010, **82**, 930–934.
3 U. Bahr, H. Aygün and M. Karas, *Anal. Chem.*, 2009, **81**, 3173–3179.
4 M. Rohmer, B. Meyer, M. Mank, B. Stahl, U. Bahr and M. Karas, *Anal. Chem.*, 2010, **82**, 3719–3726.
5 Z. Guo, Q. Zhang, H. Zou, B. Guo and J. Ni, *Anal. Chem.*, 2002, **74**, 1637–1641.
6 G. McCombie and R. Knochenmuss, *Anal. Chem.*, 2004, **76**, 4990–4997.
7 A. Tholey and E. Heinzle, *Anal. Bioanal. Chem.*, 2006, **386**, 24–37.
8 S. M. Weidner and J. Falkenhagen, *Rapid Commun. Mass Spectrom.*, 2009, **23**, 653–660.
9 J. Sunner, E. Dratz and Y.-C. Chen, *Anal. Chem.*, 1995, **67**, 4335–4342.
10 J. Wei, J. M. Buriak and G. Siuzdak, *Nature*, 1999, **399**, 243–246.
11 H. Z. Alhmoud, T. M. Guinan, R. Elnathan, H. Kobus and N. H. Voelcker, *Analyst*, 2014, **139**, 5999-6009.
12 Y.-F. Huang and H.-T. Chang, *Anal. Chem.*, 2006, **78**, 1485–1493.
13 H. Kawasaki, T. Sugitani, T. Watanabe, T. Yonezawa, H. Moriwaki and R. Arakawa, *Anal. Chem.*, 2008, **80**, 7524–7533.
14 V. Amendola, L. Litti and M. Meneghetti, *Anal. Chem.*, 2013, **85**, 11747–11754.
15 C. R. McAlpin, K. J. Voorhees, A. R. Corpuz and R. M. Richards, *Anal. Chem.*, 2012, **84**, 7677–7683.
16 R. P. Obena, P.-C. Lin, Y.-W. Lu, I.-C. Li, F. del Mundo, S. dR. Arco, G. M. Nuesca, C.-C. Lin and Y.-J. Chen, *Anal. Chem.*, 2011, **83**, 9337–9343.
17 S. Xu, Y. Li, H. Zou, J. Qiu, Z. Guo and B. Guo, *Anal. Chem.*, 2003, **75**, 6191–6195.
18 H. Zhang, S.W. Cha, and E.S. Yeung, *Anal. Chem.* **2007**, *79*, 6575–6584, *Anal. Chem.,* 2007, **79**, 6575–6584.
19 Q. Min, X. Zhang, X. Chen, S. Li and J.-J. Zhu, *Anal. Chem.*, 2014, **86**, 9122–9130.
20 M. Lu, Y. Lai, G. Chen and Z. Cai, *Anal. Chem.*, 2011, **83**, 3161–3169.
21 Y.-H. Shih, C.-H. Chien, B. Singco, C.-L. Hsu, C.-H. Lin and H.-Y. Huang, *Chem. Commun.*, 2013, **49**, 4929–4931.
22 W.-T. Chen, C.-K. Chiang, Y.-W. Lin and H.-T. Chang, *J. Am. Soc. Mass Spectrom.*, 2010, **21**, 864–867.

23 T.-C. Chiu, L.-C. Chang, C.-K. Chiang and H.-T. Chang, *J. Am. Soc. Mass Spectrom.*, 2008, **19**, 1343–1346.
24 G. Piret, D. Kim, H. Drobecq, Y. Coffinier, O. Melnyk, P. Schmuki and R. Boukherroub, *Analyst*, 2012,**137**, 3058-3063.
25 Y. Gholipour, S. L. Giudicessi, H. Nonami and R. Erra-Balsells, *Anal. Chem.*, 2010, **82**, 5518–5526.
26 X.-S. Li, J.-H. Wu, L.-D. Xu, Q. Zhao, Y.-B. Luo, B.-F. Yuan and Y.-Q. Feng, *Chem. Commun.*, 2011, **47**, 9816–9818.
27 Y. Ma, X. Zhang, T. Zeng, D. Cao, Z. Zhou, W. Li, H. Niu and Y. Cai, *ACS Appl. Mater. Interfaces*, 2013, **5**, 1024–1030.
28 K. Shrivas, S. K. Kailasa and H.-F. Wu, *Proteomics*, 2009, **9**, 2656–2667.
29 C.-K. Chiang, Z. Yang, Y.-W. Lin, W.-T. Chen, H.-J. Lin and H.-T. Chang, *Anal. Chem.*, 2010, **82**, 4543–4550.
30 X.-M. He, G.-T. Zhu, J. Yin, Q. Zhao, B.-F. Yuan and Y.-Q. Feng, *J. Chromatogr. A*, 2014, **1351**, 29–36.
31 C. Pan, S. Xu, L. Hu, X. Su, J. Ou, H. Zou, Z. Guo, Y. Zhang and B. Guo, *J. Am. Soc. Mass Spectrom.*, 2005, **16**, 883–892.
32 A. Fülöp, M. B. Porada, C. Marsching, H. Blott, B. Meyer, S. Tambe, R. Sandhoff, H.-D. Junker and C. Hopf, *Anal. Chem.*, 2013, **85**, 9156–9163.
33 S. Chen, H. Zheng, J. Wang, J. Hou, Q. He, H. Liu, C. Xiong, X. Kong and Z. Nie, *Anal. Chem.*, 2013, **85**, 6646–6652.
34 C. D. Cerruti, F. Benabdellah, O. Laprévote, D. Touboul and A. Brunelle, *Anal. Chem.*, 2012, **84**, 2164–2171.
35 N. Bao, L. Shen, Y. Wang, P. Padhan and A. Gupta, *J. Am. Chem. Soc.*, 2007, **129**, 12374–12375.
36 X. Wang, J. Zhuang, Q. Peng and Y. Li, *Nature*, 2005, **437**, 121–124.
37 M. Zhu, D. Meng, C. Wang and G. Diao, *ACS Appl. Mater. Interfaces*, 2013, **5**, 6030–6037.
38 A. Dandia, A. K. Jain and S. Sharma, *RSC Adv.*, 2013, **3**, 2924–2934.
39 J. Zheng, Z. Lin, W. Liu, L. Wang, S. Zhao, H. Yang and L. Zhang, *J. Mater. Chem. B*, 2014, **2**, 6207–6214.
40 M. Dashtiev, E. Wäfler, U. Röhling, M. Gorshkov, F. Hillenkamp and R. Zenobi, *Int. J. Mass Spectrom.*, 2007, **268**, 122–130.
41 S. Nitta, H. Kawasaki, T. Suganuma, Y. Shigeri and R. Arakawa, *J. Phys. Chem. C*, 2013, **117**, 238–245.
42 H. Sonderegger, C. Rameshan, H. Lorenz, F. Klauser, M. Klerks, M. Rainer, R. Bakry, C. Huck and G. Bonn, *Anal. Bioanal. Chem.*, 2011, **401**, 1963–1974.
43 N. Budimir, J.-C. Blais, F. Fournier and J.-C. Tabet, *Rapid Commun. mass Spectrom.*, 2006, **20**, 680–684.
44 H.-P. Wu, C.-L. Su, H.-C. Chang and W.-L. Tseng, *Anal. Chem.*, 2007, **79**, 6215–6221.
45 F. S. Tehrani, V. Daadmehr, A. T. Rezakhani, R. H. Akbarnejad and S. Gholipour, *J. Supercond. Nov. Magn.*, 2012, **25**, 2443–2455.